International Journal of Aeronautical and Space Sciences
https://doi.org/10.1007/s42405-024-00746-0

IJASS International Journal of Aeronautical and Space Sciences

ORIGINAL PAPER

Numerical Evaluation of Varying Combustion Chamber Length on the Performance of Pulse Detonation Engine Using DES Model

Arvind Pallela[1] · Shivam Kumar[2] · Amit Kumar Thakur[1] · Lovi Raj Gupta[1] · Rajesh Singh[3]

Received: 2 November 2023 / Revised: 18 April 2024 / Accepted: 20 April 2024

Abstract
A two-dimensional detached eddy simulation was performed to investigate the behavior of a detonation wavelet in a pulse detonation engine. A chemical kinetic reactive flow of acetylene and oxygen was introduced into the simulation to analyze the reactive flow dynamics of two different models. A comparative study was conducted on the detonation flow dynamics by varying the combustion chamber length. A comprehensive time-transient simulation with computation-intensive iterations was conducted to study the slightest change in the detonation wave characteristics. The results of the simulations suggest that a shorter combustion chamber in Model A provided a sustainable detonation. In comparison, Model B, with a longer combustion chamber, provided a dual detonation wave, which resulted in increased flow frequency of the detonation wave.

Keywords Pulse detonation · Combustion · Numerical simulation · Detached eddy simulation

1 Introduction

In recent years, there has been significant research interest in pulse detonation engines (PDEs) due to their potential advantages in aerospace propulsion [1]. PDEs promise higher thermodynamic efficiency, simplified design, and reduced manufacturing and operational costs compared to traditional gas turbine engines. However, several technical challenges must be addressed to make PDEs practical for real-world applications [2, 3]. Pulse detonation engine (PDE) has been in focus for its next-generation capabilities that could revolutionize aerospace. Unlike previous engines that rely on subsonic combustion or deflagration, a PDE can convert raw detonation waves into usable thrust for a spacecraft [4, 5]—resulting in less fuel and oxidizer consumption than any regular engine, which needs a steady propellant feed to achieve a nominal impulse. A typical pulse detonation engine has a specific impulse of close to 5000 s and an exit velocity of close to 2000 m/s. The specific impulse may reach an upward limit of close to 9000 s and an exit velocity of up to 4000 m/s for a pulse detonation rocket engine [6, 7]. It could translate into a notable increase in performance and a decrease in propellant consumption because of the effective conversion of potential energy to kinetic energy [8].

Though the value of the engine has been recognized, the understanding of the engine's function is still vague due to the complex nature of the detonation wave. Independently, deflagration and detonation have been understood to be forms of combustion and are well researched. However, the key concern about a PDE is the deflagration-to-detonation transition (DDT) [9, 10]. The phenomenon is not entirely understood as it involves many parameters of deflagration and detonation. Deflagration occurring within a confined space can result in an explosion. The act of confining the reaction leads to heightened pressure, an accelerated reaction rate, and increased temperature. This confinement may induce a transition to detonation. Despite the rapid and potent nature of the ensuing explosion, the combustion event unfolds as a deflagration wave traverses through the unburned reactants. The thermal energy released during the reaction sustains its progression. Importantly, combustion reaction and shock wave propagation processes proceed independently in deflagration and are not directly coupled [11–13].

Communicated by Jeong-Yeol Choi.

✉ Amit Kumar Thakur
amitthakur3177@gmail.com

[1] Lovely Professional University, Phagwara, Punjab 144001, India

[2] Department of Aerospace Engineering, Punjab Engineering College, Chandigarh, India

[3] Uttaranchal Institute of Technology, Uttaranchal University, Dehradun, Uttarakhand 248007, India

Published online: 23 May 2024

While deflagration observed in rocket engines or jet engines is rapid in scale but does not present a shock front like in the case of detonation [14]. These shock fronts are channelized by turbulence induction to convert the hazy shockwaves into usable thrust by the engine. It is achieved by introducing an obstacle in the path of the shockwaves to elevate the shock intensity and methodical arrangement for controlled results [15].

The primary role of a Shchelkin spiral is to introduce turbulence into the flow to channel it through the shock tube in the form of a stable and effective shockwave [16]. However, placing the Shchelkin spiral becomes crucial in a pulse detonation engine. The placement of the Shchelkin spiral directly affects the frequency at which the shockwave is generated [17]. The placement of the Shchelkin spiral directly affects the combustion chamber length and the blowdown section length.

One of the primary challenges in PDE research is the reliable initiation and propagation of detonation waves. Direct initiation of detonation waves requires an impractically large amount of energy, making the deflagration-to-detonation transition (DDT) approach more viable [18, 19]. In this approach, a low-energy source, such as an automotive spark plug, accelerates a flame, leading to a detonation front. The choice of fuel is critical, and while gaseous fuels such as hydrogen, acetylene, and propane have been commonly mentioned in the literature, liquid hydrocarbon fuels offer higher energy density [20–22].

Hybrid RANS-LES methods (HRLM) are designed to integrate the computational efficiency of statistical turbulence modeling (RANS) with the precision of scale-resolving simulations (LES), aiming to enhance the accuracy of predicting complex high-Reynolds number flows within practical computational limits [23]. Within the realm of approaches to couple RANS and LES [24], the detached eddy simulation (DES) [25] and its more recent iterations (DDES, IDDES) have gained widespread popularity [26]. It is primarily attributed to their ease of implementation in unstructured flow solvers and their applicability to intricate geometries and diverse flow conditions [27, 28].

1.1 Detached Eddy Simulation

The simulations in PDE so far have concentrated primarily on the k–ε, k–ω, or SST turbulence models. So far, the detached eddy simulation (DES) model has not been analyzed due to high computational costs. However, the DES model facilitates increased accuracy and versatility compared to other models. It is a hybrid model that combines both RANS (Reynolds averaged Navier–Stokes) and LES (large eddy simulation) models [23, 29]. It details the local eddy flow, crucial in investigating the flow dynamics of detonation waves propagating at a very high velocity.

The current investigation utilizes a DES model with a shear stress transport (SST) model. The model provides an improved flow separation prediction or detached eddies at a much-localized grid. Unlike other models, where the flow separation is linearized to a great extent, the DES model provides an accurate detached shear layer emanating from the boundary [30].

The base equation for the turbulence model is given by [31]

$$\frac{\mathrm{D}\rho k}{\mathrm{D}t} = \tau_{ij}\frac{\partial u_i}{\partial x_j} - \beta^*\rho\omega k + \frac{\partial}{\partial x_j}\left[(\mu + \sigma_k\mu_t)\frac{\partial k}{\partial x_j}\right] \tag{1}$$

$$\frac{\mathrm{D}\rho\omega}{\mathrm{D}t} = \frac{\gamma}{v_t}\tau_{ij}\frac{\partial u_i}{\partial x_j} - \beta\rho\omega^2 + \frac{\partial}{\partial x_j}\left[(\mu + \sigma_\omega\mu_t)\frac{\partial \omega}{\partial x_j}\right] + 2(1 + F_1)\rho\sigma_{\omega 2}\frac{1}{\omega}\frac{\partial k}{\partial x_j}\frac{\partial \omega}{\partial x_j}, \tag{2}$$

where the eddy viscosity is defined as

$$v_t = \frac{a_1 k}{\max(a_1\omega; \Omega F_2)}. \tag{3}$$

1.2 Contributions and Recommendations of the Proposed Study

The current study proposes a detailed analysis of the internal ballistics of the pulse detonation engine using detached eddy simulation. Detached eddy simulation (DES) is a new simulation method that combines the advantages of LES and RANS to provide higher accuracy with lower mesh. It is a detailed method used to study the internal ballistics, shock association, and dissociation. DES can enhance the understanding of the pulse detonation engine and shockwave transmission. However, a comprehensive study of a time-transient DES model has not been conducted yet. Therefore, the current research aims to validate the DES model for a pulse detonation engine and study the impact of the igniter's position and the combustion chamber's length on the engine's overall performance. A four times larger combustion chamber was used in the current study to observe a visible change. The present simulation focuses on the detonation engine's 2-D time-transient model. Due to the extreme computational cost necessary for a 3-D time-transient simulation, a 2-D model was selected. However, all the boundary conditions were adjusted to get an accurate simulation for the current case.

2 Experimental Setup

The experimental setup was established at Punjab Engineering College (PEC) in Chandigarh, India, comprising

three distinct sections: the combustion section, the Shchelkin section, and the blowdown section. A dynamic load cell with a sensitivity of 10 mV/lb and an upper frequency limit of 36,000 Hz was utilized for capturing dynamic measurements. The setup featured a uniform cross-sectional diameter of 48 mm and a total length of 1256 mm with a combustion chamber length of 100 mm. An integral component of the experimental apparatus was a Shchelkin spiral with a diameter of 6 mm, a pitch of 25 mm, and an overall length of 280 mm, serving a critical role in the experiments.

High-quality SS 304 steel with a thickness of 5 mm was used to build the engine. Each section was carefully insulated with gaskets to prevent any pressure leakage. Pressure transducer sensors were placed at intervals of 360 mm inside the engine to record dynamic pressure data at multiple locations. A PCB pressure sensor, in combination with a PCB piezotronics signal conditioner, is used to acquire the dynamic pressure readings. All sensors were connected to the data acquisition unit (NI-PXIe-1082), and a specialized interface was developed for the experiments using LabView. The experimental section incorporated various auxiliary components and elements into the pulse detonation engine (PDE) test rig. These experiments were executed utilizing the PDE test rig housed in the Aerospace Engineering Department at PEC in Chandigarh. The test rig featured an array of flow controllers for managing fuel and the requisite controllers for the ignition system, among other auxiliary devices, as illustrated in the schematic diagram of the PDE test rig presented in Fig. 1a.

Within this test rig, a PDE tube constructed from SS-304 grade material was meticulously designed, segmented into sections using temporary fasteners, and assembled per the necessary configuration. The first section of this tube served as the fuel-oxidizer mixing and combustion chamber, followed by the Shchelkin spiral section, which accommodated the spiral or deflagration-to-detonation transition (DDT) device, crucial for promoting detonation. The final section was the blowdown section, which guided the shock wave post-detonation towards the exhaust outlet. Comprehensive specifications of the PDE pipe are delineated.

Stop bolts were employed to secure the Shchelkin spiral firmly in place, and a thrust stand, equipped with a slider and rail system, enabled the observation of PDE movement after ignition. This setup facilitated the calculation of thrust values, and a thrust wall was utilized to support the load cell for precise thrust measurements.

Throughout the tube length, ports were strategically positioned to accommodate pressure sensors. Furthermore, separate ports were designated for fuel and oxidizer injection, situated near the dead end of the tube. Fuel and oxidizer were injected diagonally opposite each other to ensure adequate mixing. The ratio of fuel to oxidizer could be adjusted as per experimental requirements. The ignition process was executed via a spark plug integrated into the dead end of the tube.

The current study focuses on the numerical comparison of Model A and Model B. Model A has also been studied experimentally. The schematics of the Model A experiment are shown in Fig. 1a, and the outline for the Model B is presented in Fig. 1b. Model B is only a numerical model in the current study and has not been studied experimentally.

2.1 Design

The Shchelkin spiral is a critical component in pulse detonation engines (PDEs) that promote the transition from deflagration to detonation. Calculating the parameters of a Shchelkin spiral involves determining its dimensions, pitch, and diameter. The spiral pitch is the distance between successive turns of the spiral. It plays a crucial role in controlling the frequency of the shockwaves generated in the PDE. The desired frequency of the shockwaves (f) is based on the experimental requirements.

Use the formula:

$$P = \frac{c}{f}, \tag{4}$$

where P is the pitch of the Shchelkin spiral (in meters), and c is the speed of sound in the medium (in meters per second). This value depends on the specific medium and conditions in your PDE.

The Shchelkin spiral's diameter influences the shockwaves' intensity and ability to promote detonation. The diameter can be calculated using the following formula:

$$D = n \cdot P, \tag{5}$$

where D is the diameter of the spiral (in meters), and n is the number of spiral turns.

The number of turns is determined by the desired length of the spiral (L) and the pitch (P). It is calculated as

$$n = \frac{L}{P}, \tag{6}$$

where n is the number of turns, L is the desired length of the spiral (in meters), and P is the pitch of the spiral (in meters), as calculated in step 1.

Using these calculations, we can determine the dimensions of the Shchelkin spiral required for specific pulse detonation engine experiments. Remember that the actual performance and effectiveness of the spiral may also depend on factors such as the geometry of the combustion chamber, the properties of the fuel and oxidizer, and the overall engine design. Experimentation and testing may be necessary to fine-tune the spiral's parameters for optimal performance.

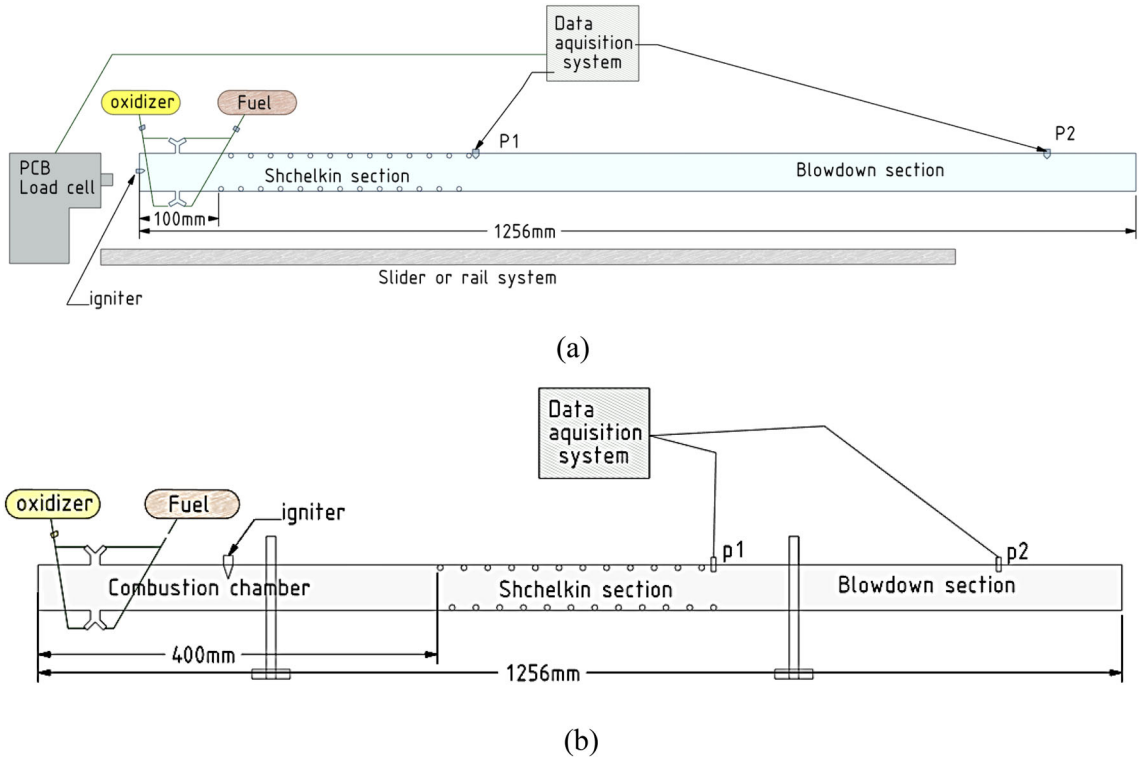

Fig. 1 **a** Schematic of the experimental setup (Model A), with a combustion chamber length of 100 mm. **b** Proposed schematic of Model B (numerical model) with a combustion chamber length of 400 mm

The blockage ratio (B) in a pulse detonation engine (PDE) is typically calculated as the total cross-sectional area blocked or occupied by various internal components and structures to the total cross-sectional area of the engine's flow path. It is expressed as a percentage. The formula for calculating the blockage ratio is as follows:

$$B = \left(\frac{A_B}{A_T}\right) \times 100\,, \tag{7}$$

where B is the blockage ratio (expressed as a percentage), A_B is the total cross-sectional area blocked or occupied by internal components and structures, such as the combustion chamber, Shchelkin spiral, instrumentation, and some obstruction. A_T is the total cross-sectional area of the engine's flow path without obstructions. The design of the two models, namely Model A and Model B, are given in Fig. 1, a, b.

3 Experimental Results

Successful experimentation was achieved by utilizing a flow control device, offering the flexibility to vary the injection timing for oxidizer and fuel, along with remote operability of ignition delay. The experiments encompassed varying tube lengths while keeping other parameters constant. For this particular experiment, a Shchelkin spiral with a length of 280 mm, a spiral pitch of 25 mm, and an outer diameter of 48 mm was selected. The Shchelkin wire diameter employed measured 6 mm. Tube lengths of 1256 mm were employed for the experimental investigations.

It is worth noting that the establishment of this test rig and the subsequent research project were driven by an exhaustive review of existing literature, which provided comprehensive insights into the characteristics of PDEs. The tube and Shchelkin spiral parameters are meticulously defined through Taguchi analysis and further optimized through systematic experimentation previously performed at Punjab Engineering College [32].

Figure 2 presents the pressure sensor readings of 2 different points. In Fig. 2a, the pressure sensor readings of point P1 are in the range of 2.1–2.3 MPa. The readings are more uniform, providing a much more stable and sustained detonation. A low-frequency detonation was used to observe the detonation initiation process and stability at the initial stage of the reaction. Figure 2b represents the pressure sensor readings of point P2. The readings are in the range of 2.2–1.5 MPa.

The current experiment has been carried out on the design of Model A, i.e., with a combustion chamber diameter of 100 mm. In Fig. 3, the reading is zoomed in to observe the reading at a very minute level. The major division of the

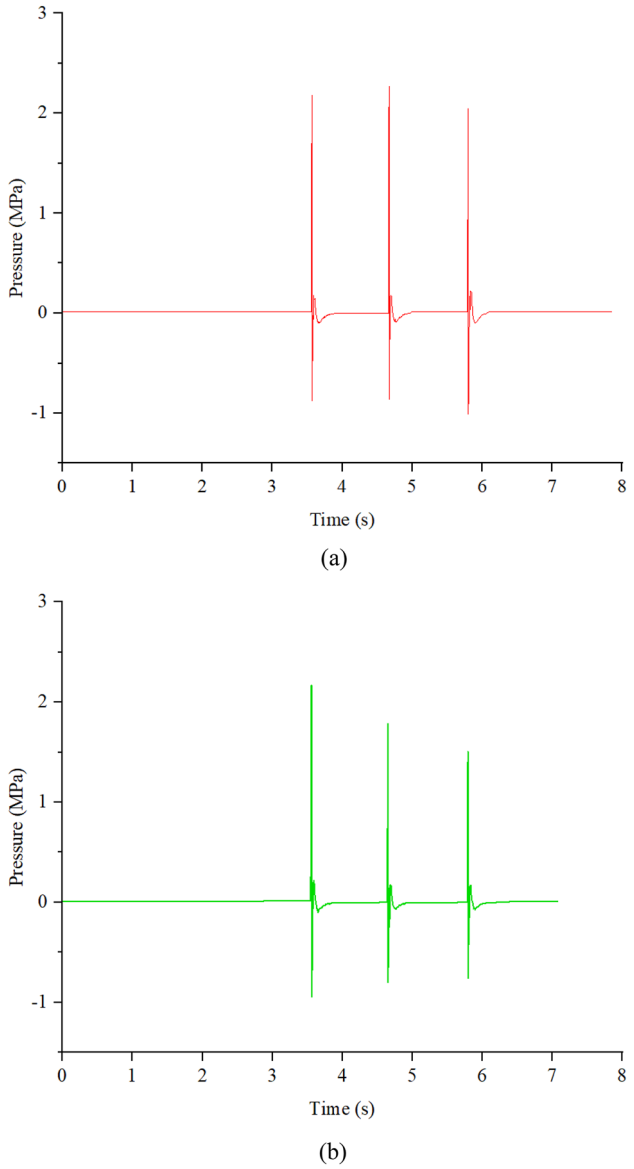

Fig. 2 Pressure sensor readings from **a** Point P1 and **b** Point P2

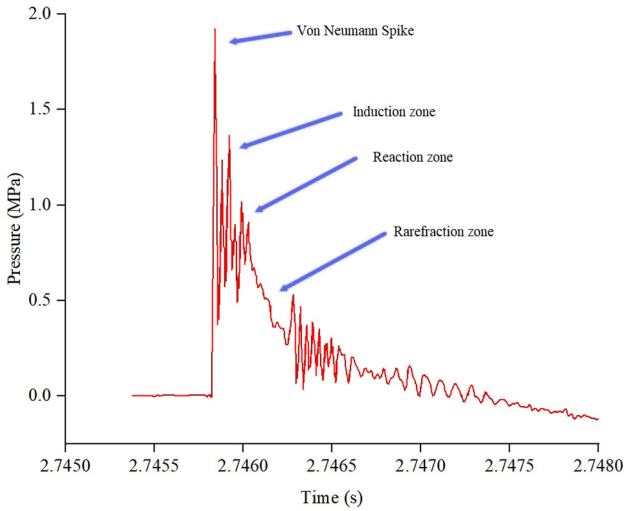

Fig. 3 Pressure readings obtained on LabView

graph is 0.5 ms on the x-axis, and 0.2 MPa is observed on the y-axis. Von Neumann Spike is observed at around 2.7458 s with the highest pressure. It is followed by the Induction zone, where the pressure drops significantly, followed by the reaction zone and rarefaction wave.

4 Numerical Model

ANSYS Fluent software is used for the current research. A large selection of general-purpose computational fluid dynamics (CFD) packages can be found in Ansys Fluent. It could be applied to a plethora of situations in numerous fields. These include simulating chemical reactions, heat, mass, and fluid flow, among other phenomena. Fluent provides a state-of-the-art, intuitive user interface that streamlines the CFD process in a single window workflow, from pre-processing to post-processing. We are using the ANSYS-16 version for this research project. There are restrictions when utilizing the student edition; for more accurate outcomes, a more significant number of mesh elements will be permitted with this licensed version.

The numerical study used a 2-D time transient, detached eddy simulation (DES) model. The internal diameter of the pulse detonation engine was maintained at 48 mm for both models. A Shchelkin spiral with a diameter of 6 mm was introduced at the exit of the combustion chamber. Model A's combustion chamber length was 100 mm, and spiral length was 280 mm, totaling 1256 mm. Model B increased the combustion chamber length to 400 mm with the same spiral and total lengths. The pitch of the Shchelkin spiral is 25 mm, the same as that of the experimental model. A fine triangular mesh was used to get accurate results. The computational load as a second-order scheme was used with a time scale factor of $1e^{-7}$ s and iterations per timestep at 250, so highly refined mesh was not used. However, the average orthogonal quality of both the Models was around 0.9, which is sufficient for the current study.

A partial non-premix ignition model with acetylene as primary fuel and oxygen as oxidizer was used. The chemistry data were obtained from the Stanford University website HyChem [33]. The Chemkin format was then imported to Ansys. The ignition points in both models were placed at different locations to assess their effect on performance simultaneously. In Model A, the ignition point was placed 13 mm from the front wall of the engine at the center. Model B's ignition point was placed 200 mm from the front wall at the center. A 5 mm inlet of fuel and oxidizer are 120º

apart to enable a homogenization of the fuel oxidizer mixture. The inlets were connected to a common inlet to inject the homogenized mixture into the combustion chamber.

A structured triangular mesh was used to improve the accuracy while maintaining the orthogonal quality close to 1. The minimum orthogonal quality obtained was 0.69. As curved sections are near the Shchelkin spiral, the adaptive mesh was used to improve mesh accuracy. A probability density function developed in the partial non-premix model gave the stoichiometry at 0.3659 mean mixture fraction weight by weight. The stoichiometry of acetylene-air is 36.59% of acetylene and 63.41% of oxygen weight by weight.

Pressure inlets were used to define the inlet boundary conditions of the fuel and oxidizer. The pressure inlet value of oxygen was 482,633 Pa, corresponding to 70 psi. Similarly, acetylene was given an inlet pressure of 206,843 Pa, corresponding to 30 Psi. This pressure combination was established to be optimum for this configuration during the experimental process. All the variables were set to second-order upwind for improved simulation accuracy. A second-order time-transient model with a time scale factor of 1e-7 s was used for the simulation. Iterations per timestep were set to 250 to ensure timestep convergence. Over 480,000 iterations were achieved for Model A and over 600,000 iterations for Model B.

5 Results and Discussion

This paper examines flow propagation and the characteristic study of flow properties. The detonation propagation in two models with different combustion chamber lengths is studied. Model A has a combustion chamber length of 100 mm, and Model B has a combustion chamber length of 400 mm. In Model A, as depicted in Fig. 1a, the igniter position is near the front end of the combustion chamber. In Model B, the igniter position is 200 mm from the front end of the combustion chamber. A comparative study of these two models is carried out to analyze the influence of combustion chamber length on the engine's performance.

An ignition charge of 50 mJ was used to ignite a mixture with a mean mixture fraction of 0.3, as 30% acetylene and 70% oxygen were used for the initial condition of both models.

5.1 Model A (Experimental)

A small combustion chamber length of 100 mm enables a rapid flow fill rate for detonation. The detonation was initiated at 1.4e-5 s, and the detonation velocity was 1430.69 m/s. A single shockwave was observed to be initiated at the front wall of the PDE. The pressurization of the detonation wave in the Shchelkin region further intensifies the velocity of the shockwave. The DES model depicts the eddy formation behind the shockwave. It can be observed in Fig. 4 that most eddies are formed around the Shchelkin region as the shockwave is propelled forward. However, as the flow propagates forward, they are diffused to a flow similar to a streamlined flow, and the entire Shchelkin acts as a Fanno tube with a uniform cross-section area. It could be safely assumed that the entire Shchelkin region acts as a nozzle throat, similar to other rocket engines. However, unlike regular rocket engines, the flow is not diffused to subsonic velocities due to the low compression ratio. The distance between two Shchelkins, instead, enables rapid contraction and expansion. It enhances the velocity of the flow further and does not allow it to reduce.

The combustion of propellant in the case of PDE is much more uniform. As can be observed in the figure, the fuel and oxidizer are injected at an angle before being injected into the combustion chamber for homogenization of the mixture. This results in the injection of premix propellant into the combustion chamber to achieve a sustainable detonation. In Fig. 5, it can be observed that the detonation propagation is much more uniform in nature, reaching close to the maximum combustion temperature of the mixture. A thin reaction layer was observed in the region of the detonation wave front, corresponding to the velocity contour. This layer has a temperature ranging from 1200 to 2500ºK. The region behind the detonation wave has a temperature over 2500 ºK.

As the reaction enters the Shchelkin region, the propellant becomes trapped between two Shchelkin spirals, causing delayed combustion due to high flow velocity. This delay further pressurizes the wave in the Shchelkin region. As the combustion propagates to the blowdown section, the thickness of the reaction wave increases exponentially due to the diffusion of pressure compared to the Shchelkin region. In addition, the flow in the blowdown section is not confined to boundaries, unlike the Shchelkin region.

From the pressure contour in Fig. 6, it can be observed that the pressure inside the combustion chamber increases as the flow propagates. The maximum pressure is observed at the Shchelkin section of the engine. A maximum pressure of 4,256,370 Pa was observed at the end of the Shchelkin section. However, the pressure over the spiral was observed to be higher. Until 0.6 μs, the flow was observed to be pressurized. After this, the flow started to diffuse in the blowdown section. The blockage created by the spiral exhibits properties similar to that of a nozzle. However, as the flow propagated to the blowdown section, it diffused the flow.

In the combustion chamber of Model A, the reaction of the propellant species is incomplete and extends into the engine's Shchelkin and blowdown section. Figure 7 shows that the reaction of acetylene and oxygen continues until the exit, forming various species. The major composition of these species is carbon monoxide (CO), hydroxide (OH), steam

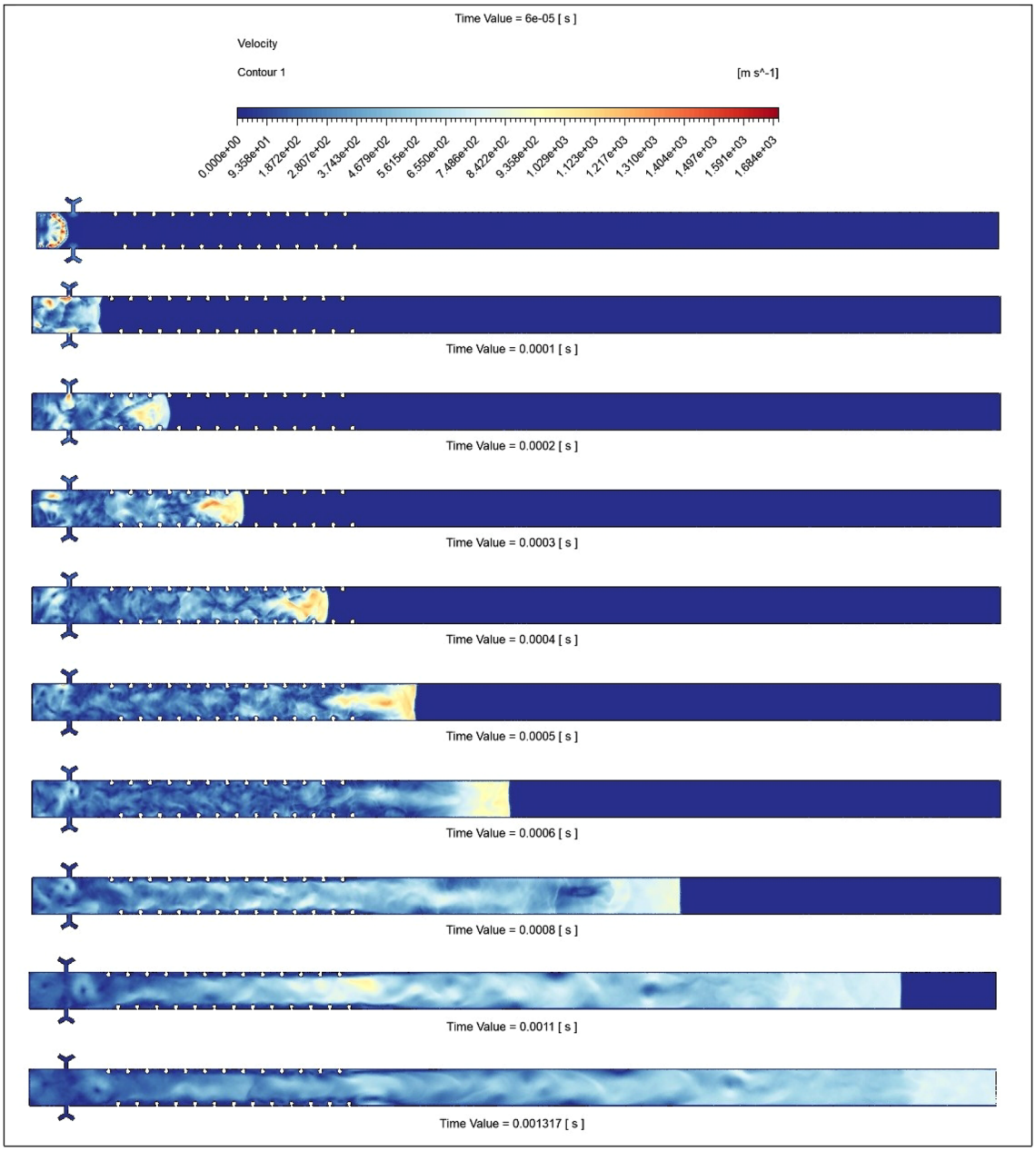

Fig. 4 Time transient velocity contour of Model-A

(H_2O), atomic oxygen (O), hydrogen gas (H_2), atomic hydrogen (H), and carbon dioxide (CO_2). However, some of these species are initially unstable and react further to stabilize, such as CO. The CO, O, and H concentrations are higher on the reaction shock layer. Behind the shockwave, these species react further to form H_2O and CO_2. Due to a shorter combustion chamber length, these reactions tend to spill into the blowdown section closer to the exit.

The reaction layer or the detonation wave velocity is closer to Mach number 1. The layer is very thin, and it could be observed from the speed of sound contour that the variation of the speed of sound is from 402 to over 1300 m/s. The Damköhler number indicates the reaction rate of flow. It could be defined as the ratio of Kolmogorov time scale to the characteristic chemical time scale. Lower values of the Damköhler number indicate a higher reaction rate. In this model, the Damköhler number is low behind the detonation wave and high in front of the wave, indicating a faster reaction rate. However, the region where the Damköhler number is greater than 200 is thicker, indicating a slower reaction rate in the detonation wave region.

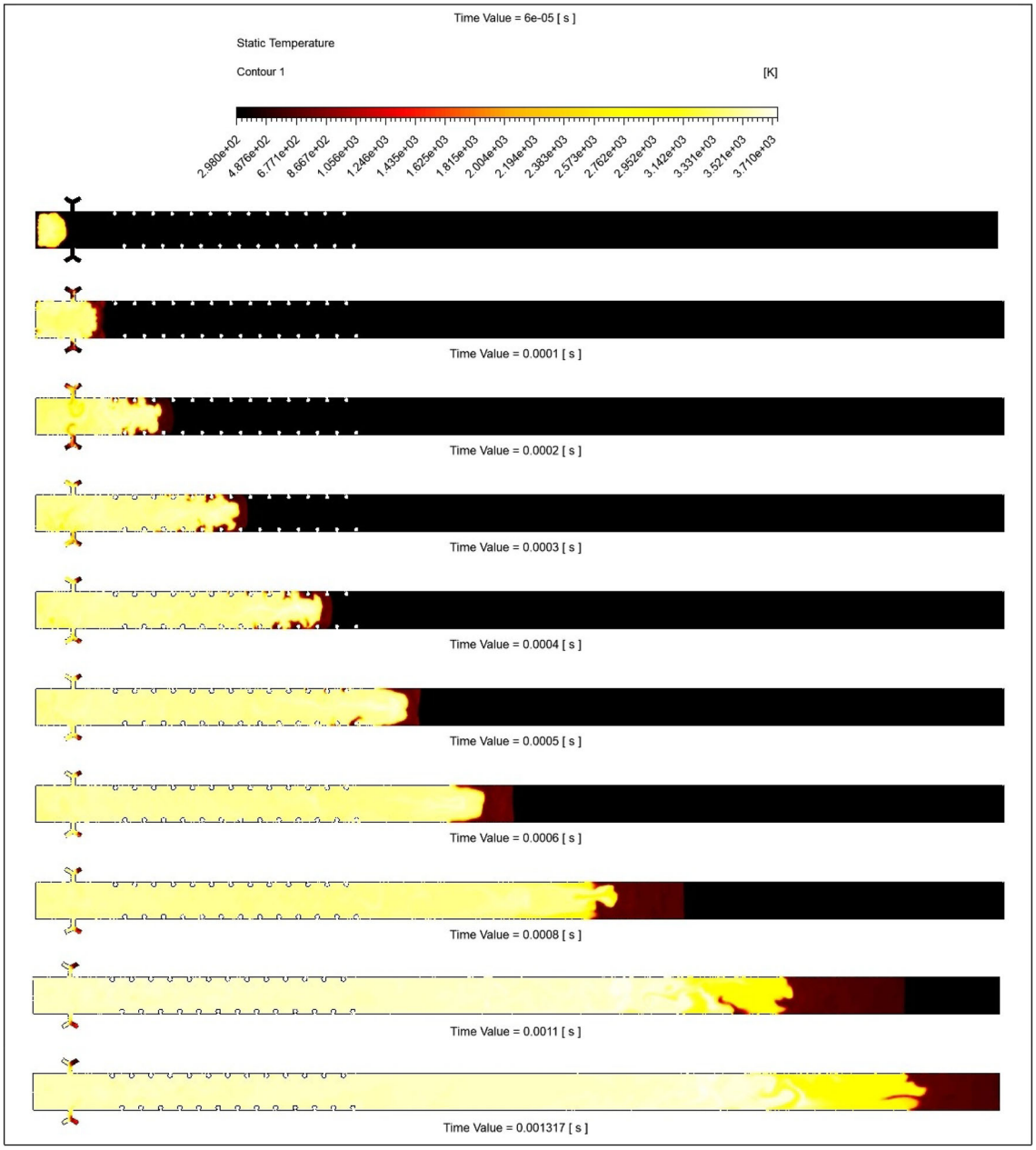

Fig. 5 Time transient Temperature contour of Model-A

5.2 Model B (Numerical)

A larger combustion chamber provides room for a more even detonation and expansion of the detonation waves. Unlike in Model A, where the detonation wave was semi-circular, the detonation wave in Model B is circular and uniform. Detonation in Model B was initiated at 1.3e–5 s, and the detonation velocity was 1625.11 m/s. After the detonation wave was triggered at the center of the combustion chamber, it was noticed that it traveled in both directions, leading to a reduction of almost 50% in the flow time for one detonation cycle while having only a slight impact on the velocity and pressure of the flow.

In contrast to Model A, the detonation in Model B was initiated at the center of the combustion chamber, resulting in two wavefronts. One wave traveled towards the exit, while the other traveled towards the closed section or front wall. The wave moving directly towards the exit exhibited properties similar to Model A's. However, a second wave reflecting on the front wall of the engine acted as a booster wave, reducing the time for the detonation wave to reach the engine exit. Velocity was higher on the detonation wavefronts, as shown

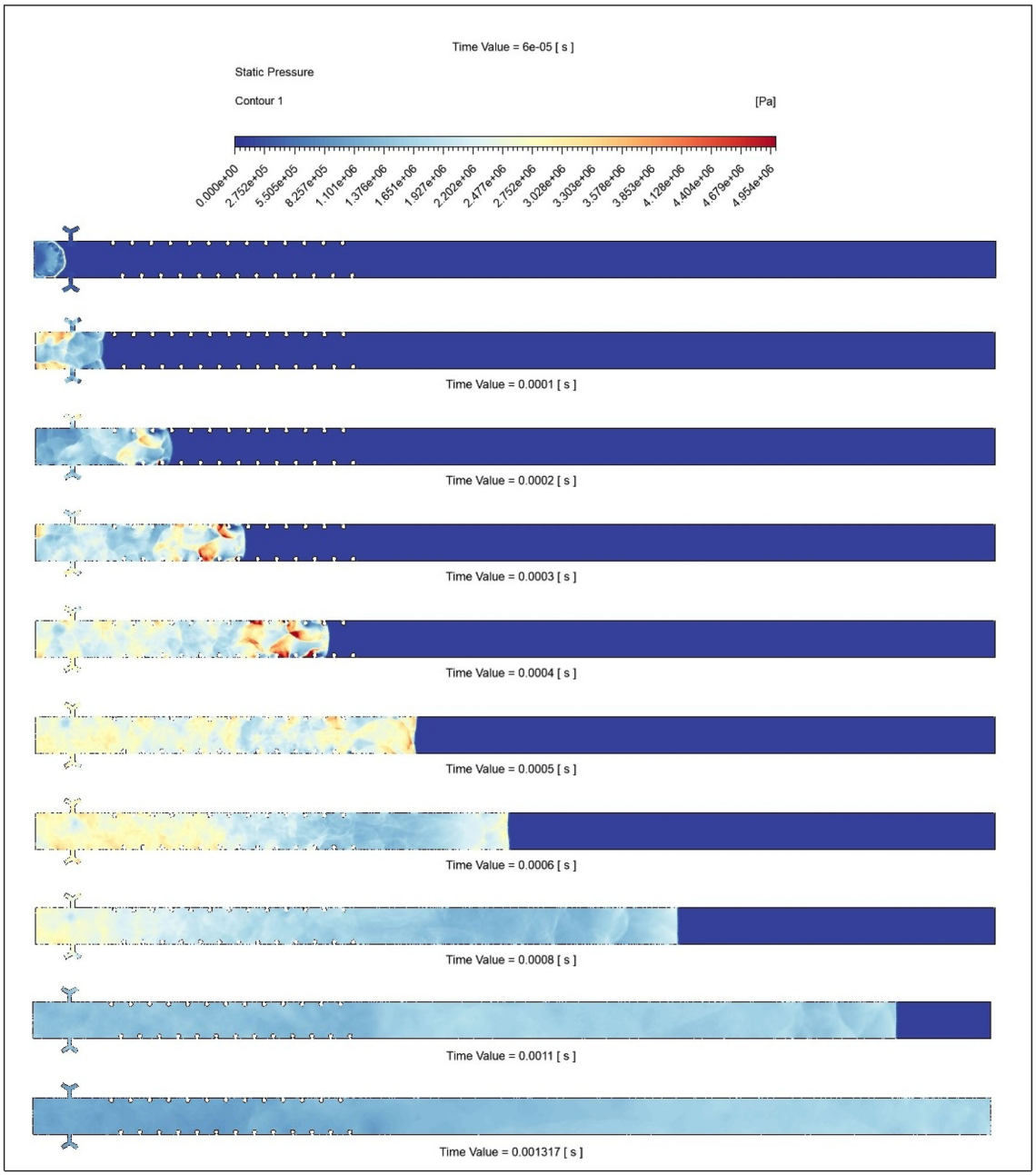

Fig. 6 Time transient Pressure contour of Model-A

in Fig. 8. Unlike Model A, where the velocity reduces substantially in the blowdown section, in Model B, the velocity is not reduced substantially, and higher velocity is maintained due to a larger combustion chamber and a reflected detonation wave, which resulted in a 13.58% increase in detonation velocity compared to Model A. In addition, the velocity propagation in the Shchelkin region was much more uniform. A zigzag pattern could also be observed more clearly in Model B due to the more uniform flow entering the Shchelkin region.

As the combustion chamber length is longer in the case of Model B, a more uniform combustion is observed. It can be observed from Fig. 9 that the reactive flow travels in dipolar form, leading to a faster combustion rate. Owing to the faster combustion of the propellant, the reaction layer thickness in the blowdown section is thinner compared to Model A. The time for completion of combustion is observed to be less than 1 μs, unlike Model B, where it is close to 50% more. However, a reduced blowdown section makes the temperature nearly 100 ºK less.

The average combustion chamber pressure is observed to be higher in Model B due to the presence of a reflective wave. From Fig. 10, it can be observed that the detonation

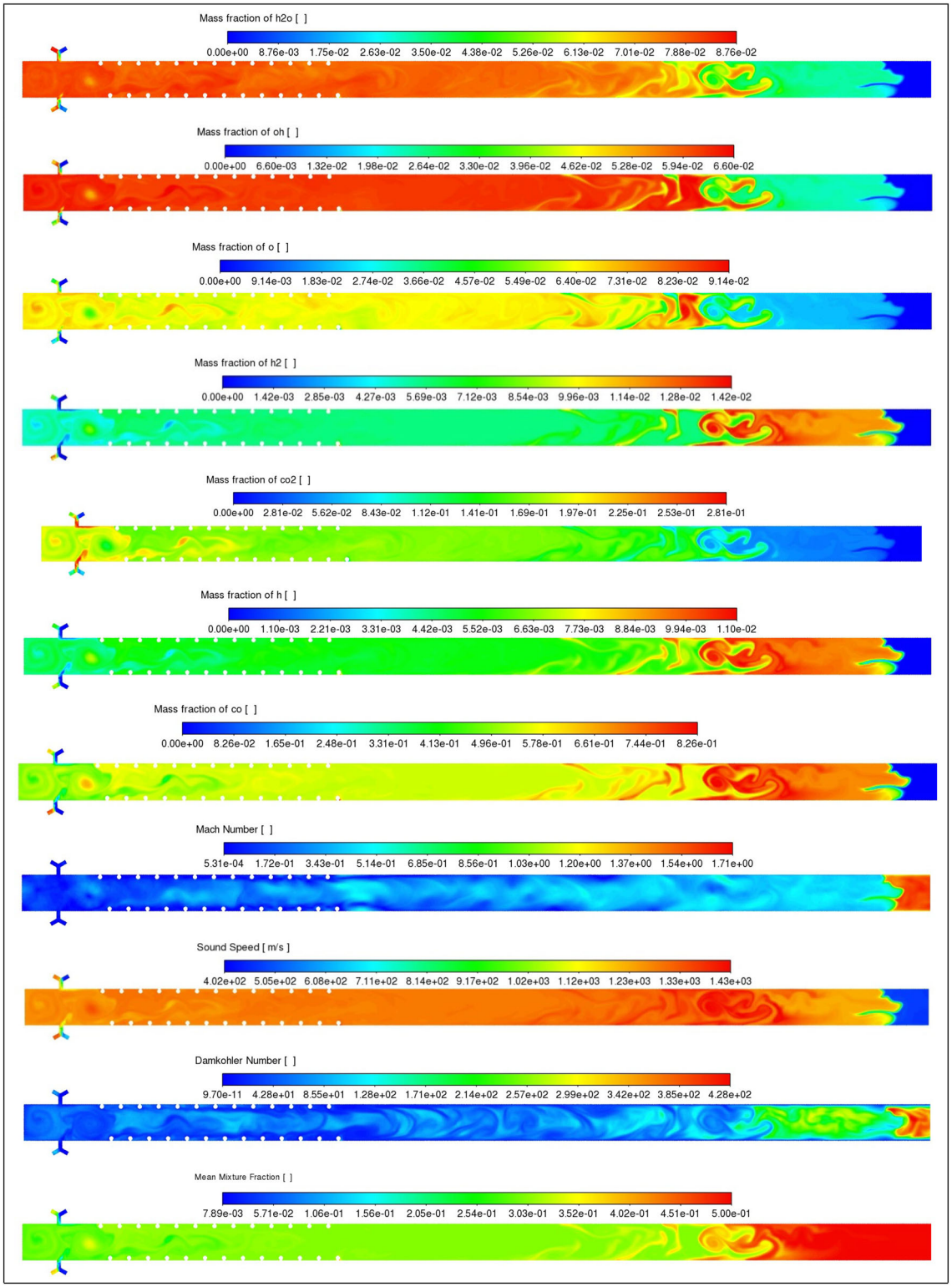

Fig. 7 Other contours of Model-A

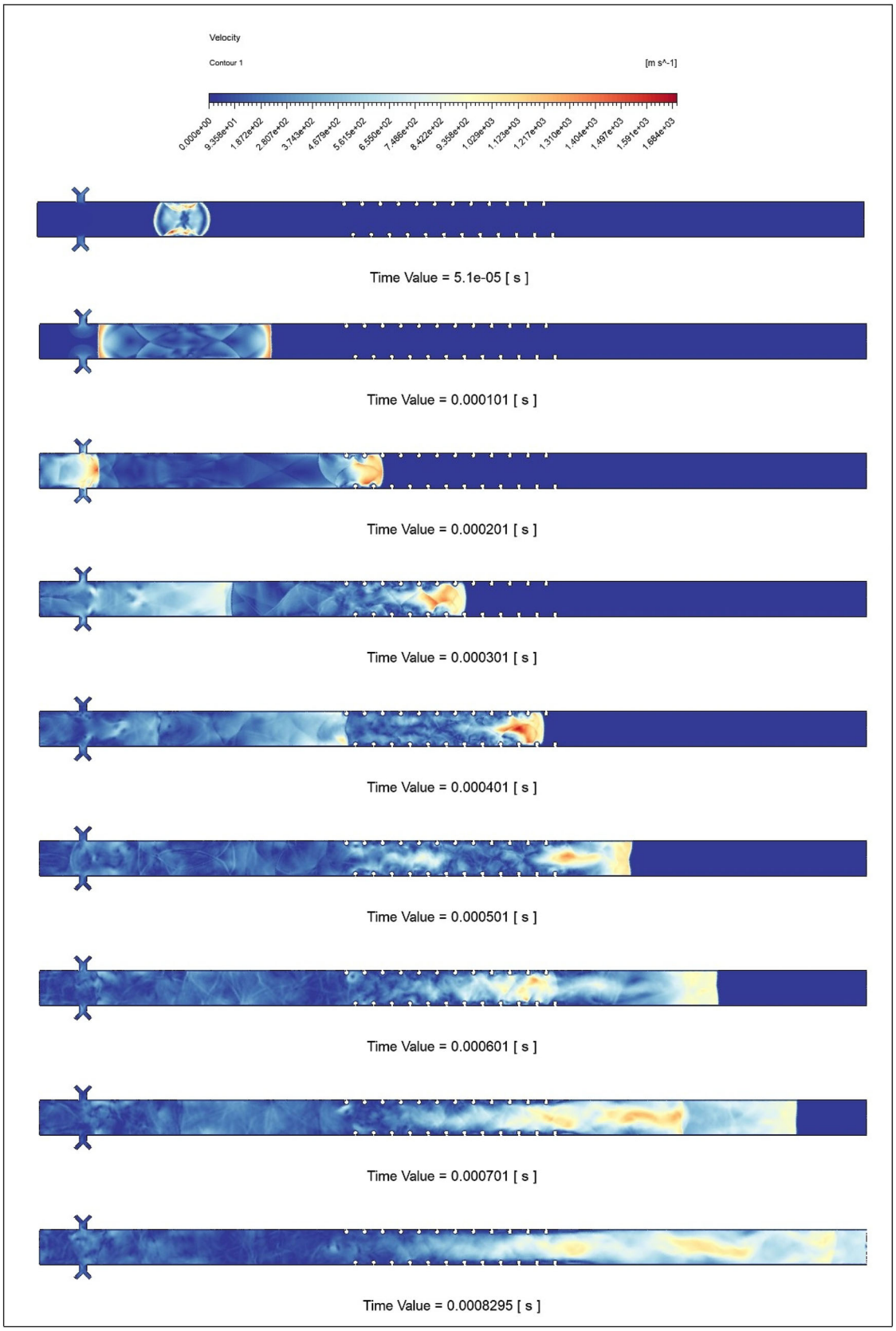

Fig. 8 Time transient velocity contour of Model-B

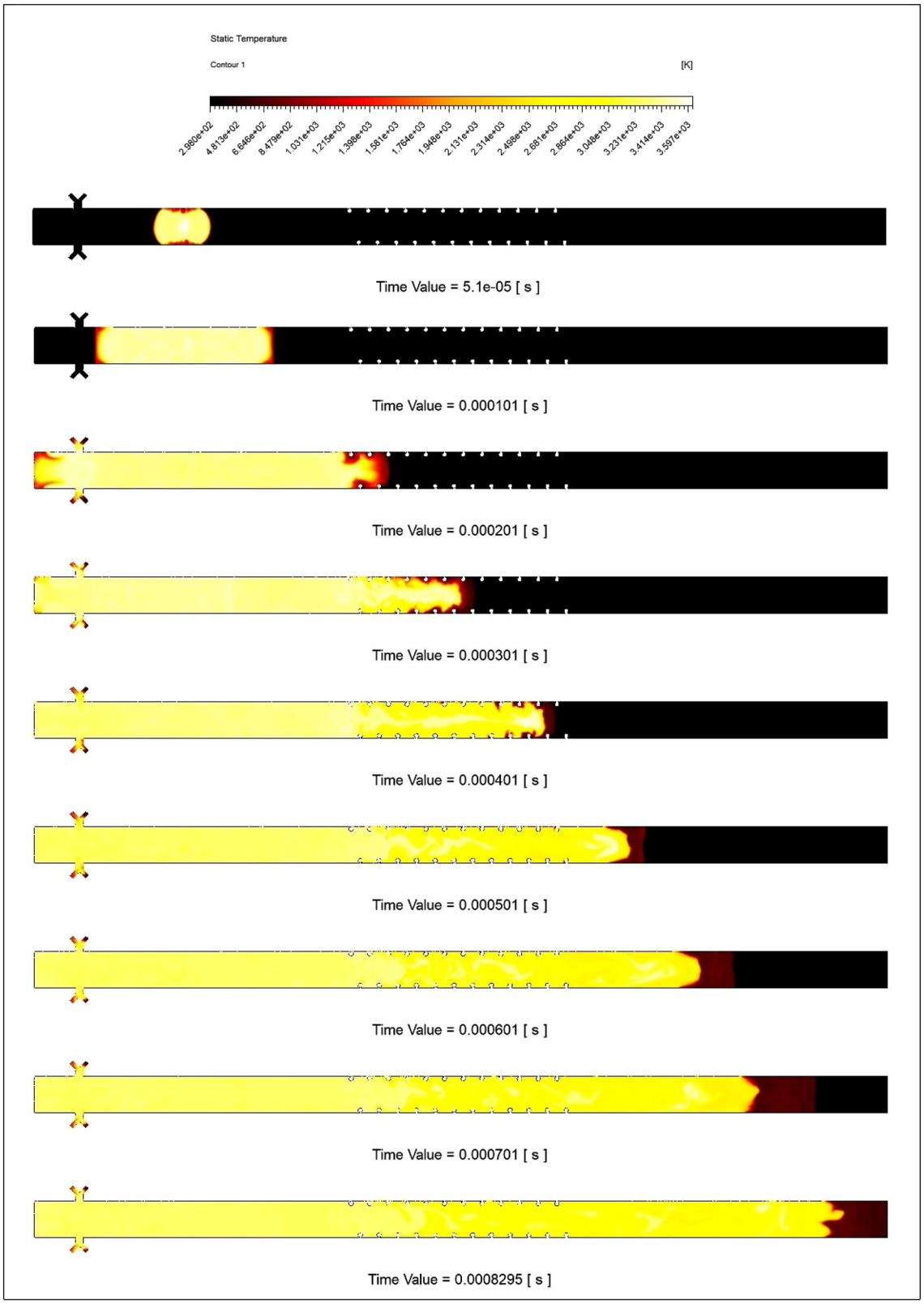

Fig. 9 Time transient Temperature contour of Model-B

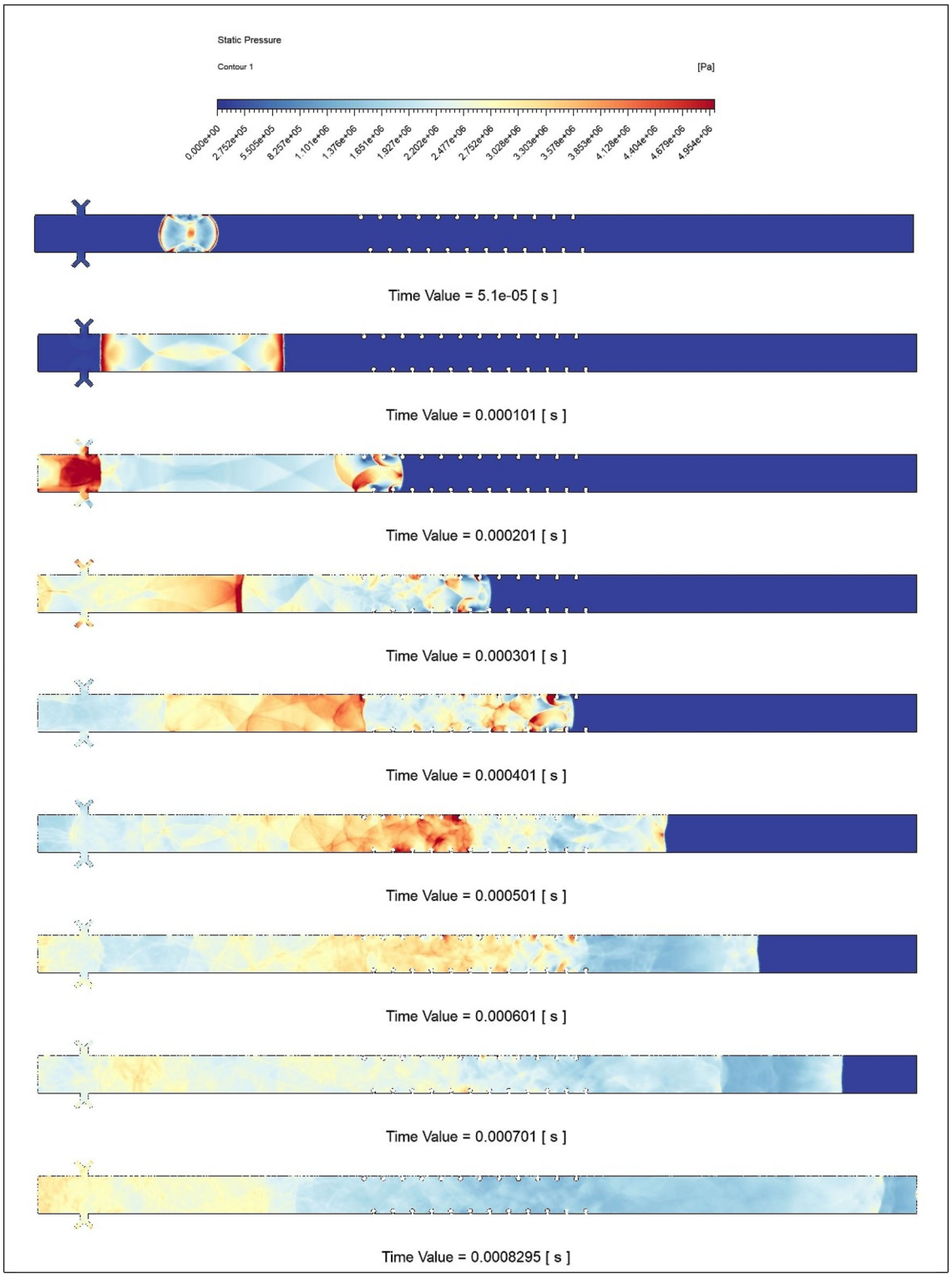

Fig. 10 Time transient Pressure contour of Model-B

wave that is propagating toward the wall compresses the propellant against the wall, increasing the combustion chamber pressure. The flow propagated towards the exit creates a low-pressure region behind the detonation wave. The detonation wave that strikes the front wall has 2–3 times higher pressure than this region. It enables re-pressurization of the combustion chamber and propagation of a second detonation wave within the same detonation cycle.

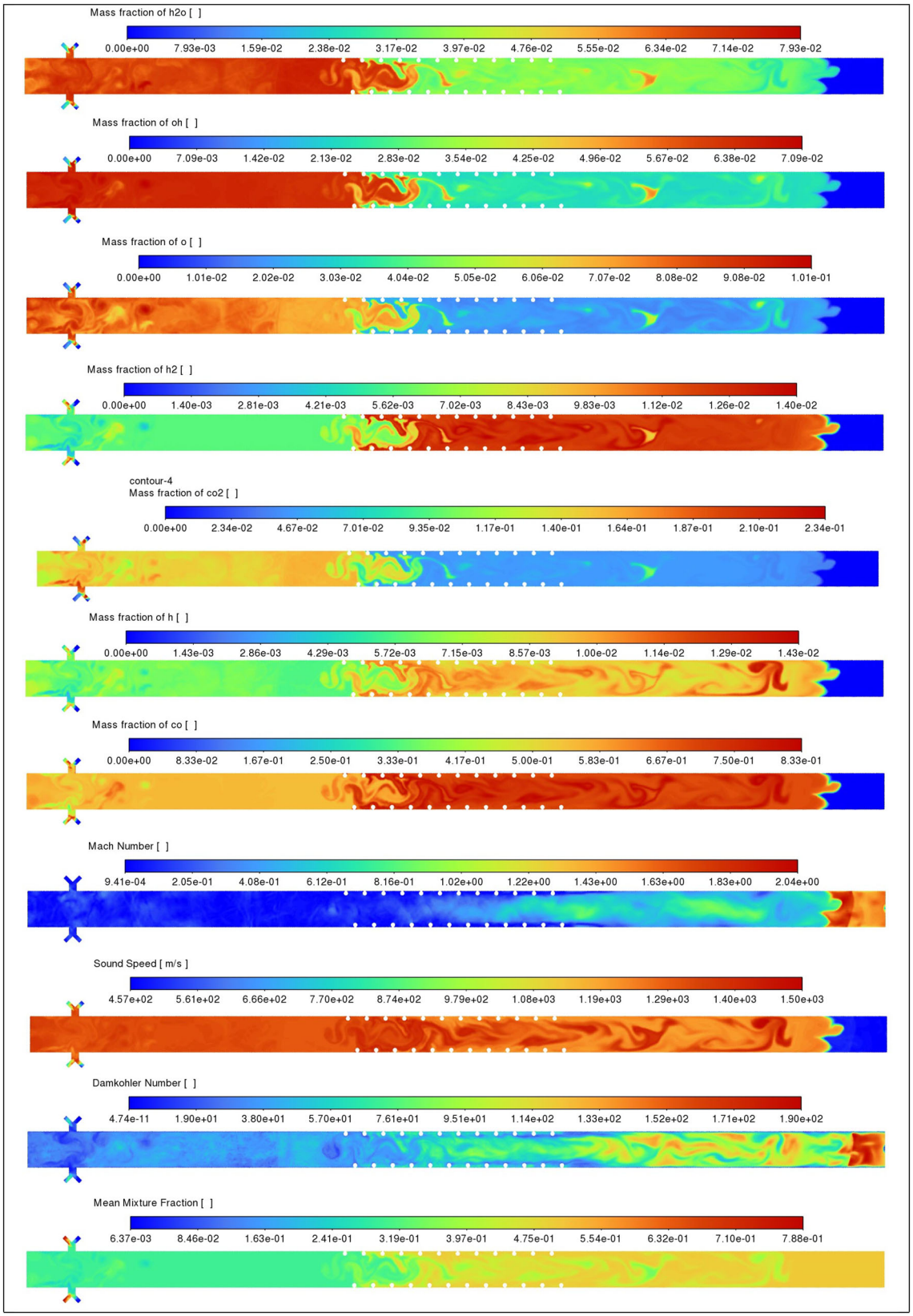

Fig. 11 Other contours of Model-B

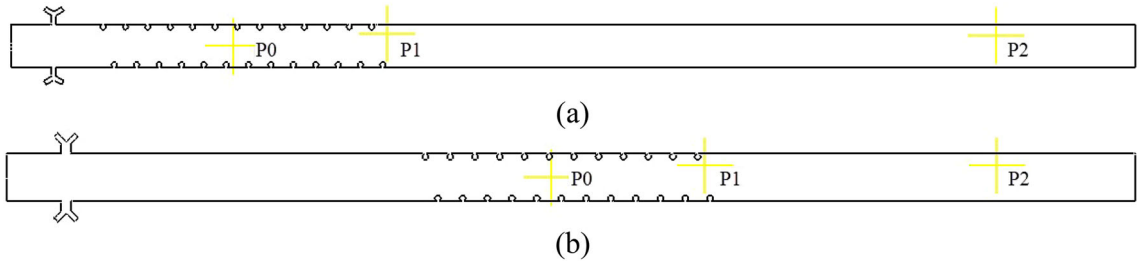

Fig. 12 Selection of points for the comparative study: **a** Model A, **b** Model B

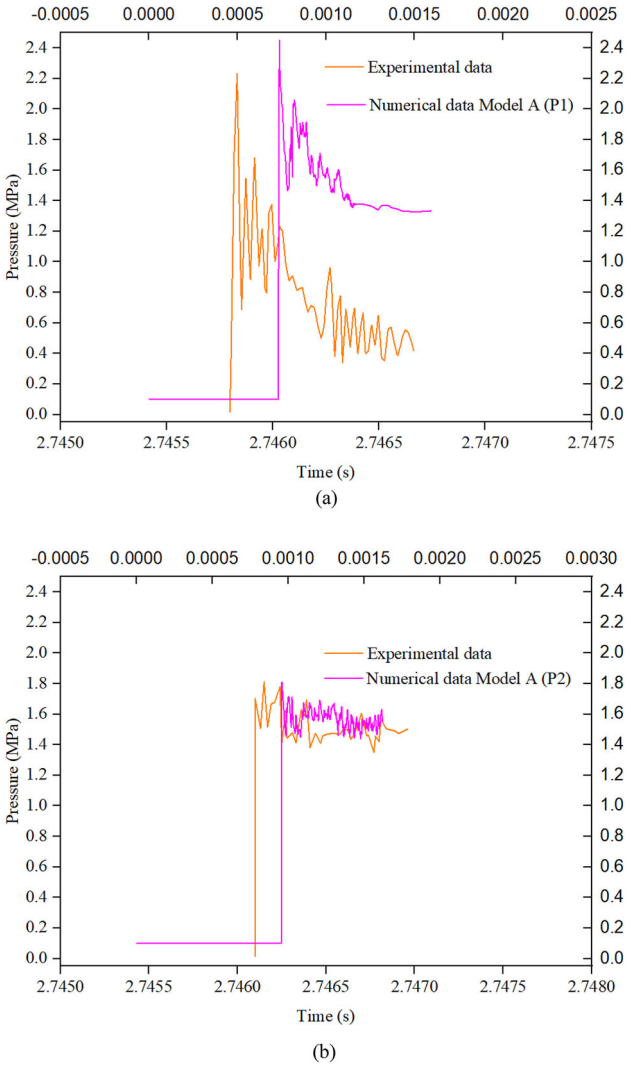

Fig. 13 Comparison of numerical and experimental pressure data at **a** point P1 and **b** point P2

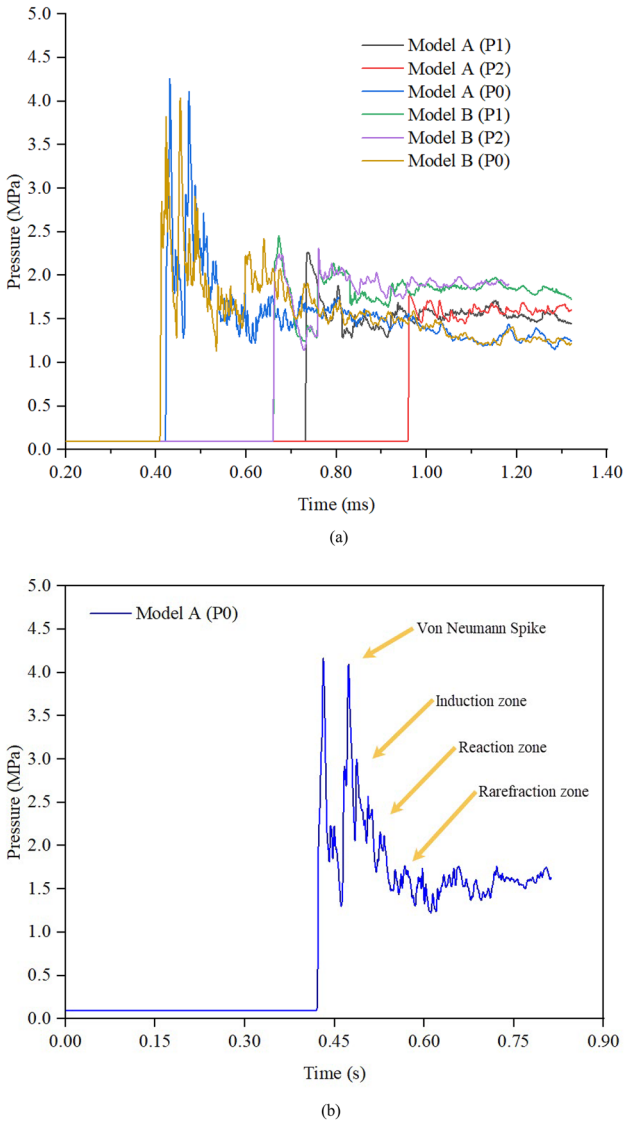

Fig. 14 **a** Comparison of pressure inside the Shchelkin region and outside the Shchelkin region. **b** The flow regime of the numerical pressure data

As more pressure is added to the supersonic flow, the second detonation wave travels faster than the first. It could be observed that even though the second wave travels close to 400 mm more than the first wave, the margin between both waves is less than 200 mm when the flow reaches the exit. It presents a crucial advantage as two detonation waves are created in the same cycle with similar exit flow properties and indicate doubling the frequency of exit flow, thereby increasing the thrust and specific impulse of the engine.

The species contours observed in Model B vary from Model A in Fig. 11. The concentration of reaction flow species observed in the combustion chamber differs from that past the Shchelkin region. It may be due to the reflected detonation wave observed in Model B. Although the reaction of the propellant has already been carried out initially, the reflected wave acts as a second wave of reaction, stabilizing the chemical reaction. A complete combustion is indicated in the combustion chamber, which indicates an almost partial vacuum in the Mach number contour, where the Mach number in the combustion chamber is close to zero. However, compared to Model A, the reaction later Mach number is higher, reaching around Mach 2. The speed of sound in the medium is also higher, indicating an increased flow density.

Damköhler's contour is much more uniform in the blowdown region, indicating a uniform reaction rate. The reaction layer Damköhler number is also low, meaning a faster reaction than Model A. However, Model A has a much more complete reaction than Model B.

6 Comparative Analysis

Both models were compared at 3 points to get an accurate insight into the numerical simulation. The points can be observed in Fig. 12. Point P1 is placed at the exit of the Shchelkin section, and this is also the point at which the pressure sensor is placed in the experimental setup. Point P2 is placed closer to the exit of the PDE, marking the placement of the second pressure sensor. These results match the corresponding results to validate the simulation of Model A. Another point, P0, is taken at the center of the Shchelkin section to study the detonation to deflagration transition properties in the Shchelkin region. The point is taken only numerically, as taking a pressure reading at the center of the Shchelkin spiral is not feasible.

The pressure data of point P1 in Model A present data and trends similar to those in Fig. 13a. The peak pressure obtained from the simulation at point P1 for Model A is 2.446 MPa, and the experimental data obtained is 2.1–2.3 MPa. In Fig. 13a, the peak pressure measurement is observed to be 2.22 MPa, with a deviation of 8.94%. The deviation between the experimental and the numerical data ranges from 6% to 14.17%. The timeline of the experimental data is represented at the bottom of the chart, and the numerical data is at the top of the chart in Fig. 13a, b. Figure 13b represents the pressure data of point P2. The numerical peak pressure was observed to be 1.809 MPa, and the experimental peak pressure was observed to be around 1.79 MPa. The deviation of peak pressure was observed to be less than 1%. However, the pressure at point P2 is varying during the course of the experiment and was in the range of 2.18–1.56 MPa. Hence, the simulation can be validated with the experimental data.

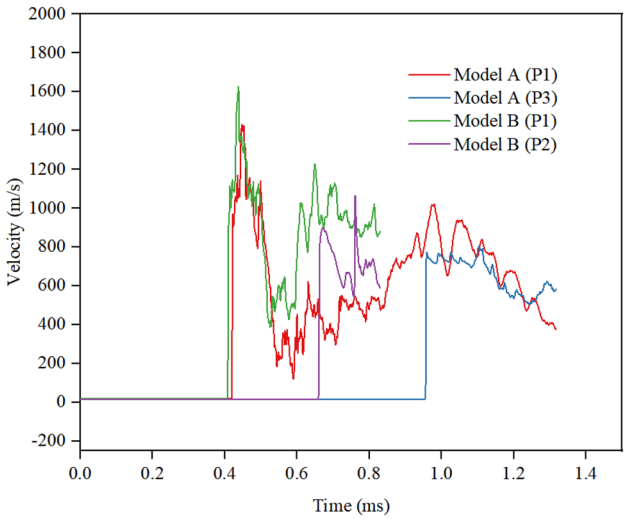

Fig. 15 Comparison of velocity profiles at the post-Shchelkin region and exit

It could be observed that the trend of pressure data is similar for both Model A and Model B in Fig. 14a. However, the graph shows that the pressure inside the Shchelkin region is higher for Model A, whereas the pressure post the Shchelkin region is higher for Model B. At both points, the pressure drops steadily after some time. However, the pressure increases again in Model B due to the second shockwave. The detonation wave flow regime inside the Shchelkin region is observed to have two pressure spikes of close to 4 MPa. The two pressure spikes are primarily due to the overlapping of the shockwaves in the Shchelkin region. The regimes of the pressure are explained in Fig. 14b. It could be observed that the Von Neumann spike is followed by the induction zone, reaction zone, and the rarefaction wave immediately.

The velocity profiles of the two models in Fig. 15 indicate a longer time for the detonation wave to reach the exit for Model A. The velocity of the wave in Model B is found to be higher along both points. The graph indicates the rise in velocity after the detonation wave has passed the point, indicating a second shockwave of velocity over 1100 m/s in Model B. The gap between the two spikes is minimal.

7 Conclusion and Future Scope

The length of the combustion chamber and the position of the ignition point significantly affect the propagation of the detonation wave in the PDE. From the current study, it could be safe to conclude that Model B presents a more viable design than Model A. The performance parameters of Model B tend to indicate a better performance than Model A. The pressure readings taken from a point outside the Shchelkin region show an improved performance of 13% for Model

B over Model A. In addition, the velocity improvement in Model B is observed to be 14%. The overall combustion regime in Model A is more sustained than Model B's.

The length of the combustion chamber heavily influences the detonation flow parameters. A duel shockwave observed in Model B tends to boost the performance of the PDE. Two shockwaves transmitting in the same cycle improve not just the performance but also the frequency. The flow fill rate improvement increases the overall efficiency of the engine. Hence, using a longer combustion chamber and initiating the ignition at the center of the combustion chamber is prudent to improve the engine's overall efficiency.

Acknowledgements We thank Lovely Professional University, Phagwara, and Jalandhar for all their support.

Funding Not applicable.

Data availabilty Not applicable

Declarations

Conflict of Interest The authors declare that they have no competing interests.

References

1. Kailasanath K (2003) Recent developments in the research on pulse detonation engines. AIAA J 41(2):145–159. https://doi.org/10.2514/2.1933
2. Valli DM, Jindal DRTK (2014) Pulse detonation engine: parameters affecting performance. Int J Innov Res Sci Eng Technol
3. Li J, Fan W, Qiu H, Yan C, Wang Y-Q (2010) Preliminary study of a pulse normal detonation wave engine. Aerosp Sci Technol 14(3):161–167. https://doi.org/10.1016/j.ast.2009.12.002
4. Liu L, Zhang Q (2019) Numerical study of cellular structure in detonation of a stoichiometric mixture of vapor JP-10 in air using a quasi-detailed chemical kinetic model. Aerosp Sci Technol 91:669–678. https://doi.org/10.1016/j.ast.2019.07.017
5. Wolaski P (2011) Detonation engines. J KONES Powertrain Transp Vol. 18, No. 3, 2011. Retrieved 6 February 2023. http://arc.uta.edu/research/pde.htm. Accessed 6 Feb 2023
6. Roy G (2006) Combustion processes in propulsion. Elsevier. https://doi.org/10.1016/B978-0-12-369394-5.X5000-8
7. Koshy P (2008) The development and testing of pulsed detonation engine ground demonstrators By," 2008. Retrieved 6 February 2023
8. Endo T, Fujiwara T (2002) A simplified analysis on a pulse detonation engine model. Trans Jpn Soc Aeronaut Sp Sci 44(146):217–222. https://doi.org/10.2322/TJSASS.44.217
9. Zhang Q, Qiao X, Fan W, Wang K, Tan F, Wang J (2020) Study on operation and propulsion features of a pulse detonation rocket engine with secondary oxidizer injection. Appl Therm Eng 180:115661. https://doi.org/10.1016/j.applthermaleng.2020.115661
10. Zhang Q, Wang K, Wang J, Qiao X, Fan W (2021) Experimental research on vector control features of a pulse detonation tube with fluidic nozzle. Aerosp Sci Technol 116:106456. https://doi.org/10.1016/j.ast.2020.106456
11. Glassman I, Yetter RA, Glumac NG (2015) Combustion. Elsevier. https://doi.org/10.1016/C2011-0-05402-9
12. Kinney GF, Graham KJ (1985) Explosive shocks in air. Springer, Berlin, Heidelberg. https://doi.org/10.1007/978-3-642-86682-1
13. Coleman ML (2001) Overview of pulse detonation propulsion technology. Chemical propulsion information agency columbia md, Technical rept. for 1942–1999
14. Dunn IB, Malik V, Flores W, Morales A, Ahmed KA (2021) Experimental and theoretical analysis of carbon driven detonation waves in a heterogeneously premixed rotating detonation engine. Fuel 302:121128. https://doi.org/10.1016/j.fuel.2021.121128
15. Fan Z-C, Fan W, Tu H, Li J-L, Yan C (2012) The effect of fuel pretreatment on performance of pulse detonation rocket engines. Exp Thermal Fluid Sci 41:130–142. https://doi.org/10.1016/j.expthermflusci.2012.04.007
16. Kublik D, Kindracki J, Wolański P (2019) Evaluation of wall heat loads in the region of detonation propagation of detonative propulsion combustion chambers. Appl Therm Eng 156:606–618. https://doi.org/10.1016/j.applthermaleng.2019.04.084
17. Wang Y, Dong R, Shen S, Li Q, Lei Q, Fan W (2021) Effect of fill flow rate on flame acceleration in a detonation channel. Aerosp Sci Technol 117:106936. https://doi.org/10.1016/j.ast.2021.106936
18. Wang Z, Wang Y, Huang J, Qin W, Wei L, Liu Z, Peng C (2021) Back-propagation suppression study based on intake configuration optimization for an air-breathing pulse detonation engine. Aerosp Sci Technol 118:107042. https://doi.org/10.1016/j.ast.2021.107042
19. Wang Z, Qin W, Huang J, Wei L, Wang Y, Zhang L, Liu Z (2021) Experimental study on the temperature and structure of the exhaust plume in valveless pulse detonation engines. Aerosp Sci Technol 117:106907. https://doi.org/10.1016/j.ast.2021.106907
20. Lin L, Hu S, Hu Y, Xu G, Jiao H, Weng C (2020) Experimental study on the detonation process of a pulse detonation engine with ionized seeds. Defence Technol 16(1):178–187. https://doi.org/10.1016/j.dt.2019.09.006
21. Wang Z, Qin W, Huang J, Wei L, Yang Y, Wang Y, Zhang Y (2022) Numerical investigation of the effect of jet intensity from internal jet tube on detonation initiation characteristics. Int J Hydrogen Energy 47(28):13732–13745. https://doi.org/10.1016/j.ijhydene.2022.02.114
22. Wang Y, Le J (2021) A rotating detonation engine using methane-ethylene mixture and air. Acta Astronaut 188:25–35. https://doi.org/10.1016/j.actaastro.2021.07.019
23. Herr M, Radespiel R, Probst A (2023) Improved delayed detached eddy simulation with reynolds-stress background modelling. Comput Fluids. https://doi.org/10.1016/j.compfluid.2023.106014
24. Fröhlich J, von Terzi D (2008) Hybrid LES/RANS methods for the simulation of turbulent flows. Prog Aerosp Sci 44(5):349–377. https://doi.org/10.1016/j.paerosci.2008.05.001
25. Spalart PR (2021) Hybrid RANS-LES methods. In: Advanced approaches in turbulence. Elsevier, pp 133–159. https://doi.org/10.1016/B978-0-12-820774-1.00010-0
26. Shur ML, Spalart PR, Strelets MKh, Travin AK (2008) A hybrid RANS-LES approach with delayed-DES and wall-modelled LES capabilities. Int J Heat Fluid Flow 29(6):1638–1649. https://doi.org/10.1016/j.ijheatfluidflow.2008.07.001
27. Masini L, Timme S, Peace AJ (2020) Scale-resolving simulations of a civil aircraft wing transonic shock-buffet experiment. AIAA J 58(10):4322–4338. https://doi.org/10.2514/1.J059219
28. Probst A, Melber-Wilkending S (2022) Hybrid RANS/LES of a generic high-lift aircraft configuration near maximum lift. Int J Numer Meth Heat Fluid Flow 32(4):1204–1221. https://doi.org/10.1108/HFF-08-2021-0525

29. Menter FR, Kuntz M, Langtry R (2003) Ten years of industrial experience with the SST turbulence model. Proceedings of the 4th International Symposium on Turbulence, Heat and Mass Transfer, Begell House Inc., West Redding, pp 625–632
30. Baurle RA, White JA, Drozda TG, Norris AT (2020) Vulcan-CFD theory manual: Ver. 7.1.0. Tech. Rep. NTRS Report Number TM-2020-5000766, Hampton, VA
31. Menter FR (1994) Two-equation eddy-viscosity turbulence models for engineering applications. AIAA J 32(8):1598–1605. https://doi.org/10.2514/3.12149
32. Mahaboob Valli, D, Jindal TK (2014) application of taguchi method for optimization of physical parameters affecting the performance of pulse detonation engine. Vol 1, No 1, 2014, pp 18–23. http://www.krishisanskriti.org/jbaer.html Accessed 8 Dec 2022
33. Download | HyChem Model. Retrieved 24 January 2024. https://web.stanford.edu/group/haiwanglab/HyChem/pages/download.html. Accessed 24 Jan 2024